Signatures of Majorana zero-modes in nanowires, quantum spin Hall edges, and quantum dots

Mi, S.

Chapter 2

Impact of the soft induced gap on the Majorana zero-modes in semiconducting nanowires

2.1 Introduction

In a recent paper Mourik *et al.* reported observing signatures of Majorana zero-modes in indium antimonide nanowires contacted by NbTiN superconductor [1] by implementing an earlier theoretical proposal [2, 3]. More specifically they have reported a zero bias peak in Andreev conductance appearing when magnetic field was applied parallel to the wire. Since creating and observing Majorana zero-modes is a long-standing challenge, this result together with follow-up experiments [4–6] has created a big interest both in the theoretical [7] and experimental communities [8].

The observations reported in Ref. 1 differ significantly from what is expected within a simple theoretical picture. In particular the appearance of the zero bias peak was not accompanied by the closing of the observed induced superconducting gap. The magnetic field at which the zero bias peak appeared was approximately a factor of two smaller than the expected value.

Perhaps the observed feature that is most hard to reconcile with existence of Majorana zero-modes is the fact that the tunneling conductance did not follow the prediction of BTK theory [9], and instead a soft gap was observed with tunneling conductance inside the gap roughly proportional to the bias voltage, or the excitation energy. Since Majorana

zero-modes are protected exactly by the superconducting gap, it is not clear whether they may appear without this protection.

The aim of our work is to figure out whether the observed soft gap may be due to low disorder in the nanowire and the presence of multiple one-dimensional bands. It is well known [10] that the broad distribution of dwell times in such integrable systems leads to a soft gap since different quasiparticles bounce off the superconductor with very different frequencies. Our conclusion is mixed: on one hand we indeed find that the multiband origin of the soft induced gap fits the observations reasonably well. If it is indeed the reason for appearance of the soft gap, this allows us to put an upper bound on the amount of disorder in the nanowire, and to conclude that disorder is not prohibitively strong to observe Majorana zero-modes. On the other hand, presence of bands with minute band gap diminishes greatly the topological protection of Majorana zero-modes and makes the nanowire implementations not directly suitable to observe the non-Abelian properties of Majorana zero-modes.

The layout of this chapter is as follows. In Sec. 2.2 we provide general considerations for the mechanism behind the induced gap. We discuss the methods we use in detail in Sec. 2.3. We describe the profile of the induced gap in Sec. 2.4, which is followed by the discussion of the relation between the soft gap and Majorana zero-modes in Sec. 2.5. We conclude in Sec. 2.6.

2.2 Possible origins of the soft gap

The superconducting hard gap in presence of time reversal symmetry is protected by Anderson's theorem [11], that shows that the gap size is not sensitive to disorder and spin-orbit interaction. There are several ways in which the Anderson theorem can be violated in the nanowire-superconductor hybrid structure.

First of all, the time reversal symmetry may be broken even in the absence of magnetic field due to the presence of magnetic impurities. Such impurities may create a fluctuating magnetic field that may suppress the superconducting gap [12]. This scenario requires the scale of the effective magnetic field created by the impurities to be tuned to the size of the superconducting gap, since otherwise either the effect of the impurities on the density of states is negligibly, or the gap completely

closes instead of acquiring a liner profile in the density of states.

The density of states may also become nonzero at low energies due to the thermal level broadening [13]. Applied to the typical experimental setup, this requires the electron temperature to be comparable to the induced superconducting gap $\sim 1K$, while most of the experiments are performed at a much lower temperature $\lesssim 100mK$, and resolve features of the much narrower width. Therefore we will focus on the low temperature regime.

Additionally, if the coupling between the normal metal and the superconductor is not weak, the differential conductance profile may get a scaling different from that of the density of states [9, 13]. Since the softness of the gap is observed to persist in the weak coupling regime $G \ll e^2/h$, we focus on the physical effects that directly modify the density of states in the nanowire.

In a hybrid system, the situation becomes more complicated, where one distinguishes the long junction junction regime when the Thouless energy $E_{\mathrm{Th}} \ll \Delta$ or the short junction regime $E_{\mathrm{Th}} \gg \Delta$. In the short junction regime most of the weight of the wave function of the Andreev states is inside the superconducting region, so that the Anderson theorem is fulfilled, and there is no modification of the BCS density of states. In the long junction regime, on the other hand, most of the weight of the Andreev state is in the normal region, so that the energy of each Andreev state is inverse of its dwell time in the normal region. Since the overall size of the observed induced gap is suppressed compared to the bulk gap in the corresponding superconductors, it is reasonable to assume that the long junction limit applies.

In order to generate a smooth profile of the overall density of states, a power law distribution of flight times towards the superconductor is required. This may be obtained in a diffusive system, with the mean free path much shorter than the distance to the superconductor [14]. Since the nanowires are nearly ballistic before depositing the superconductor, and since even the wave length in the nanowire is not much shorter than the wire diameter, this limit probably does not apply. On the other hand, when the mean free path is very long, such that the system becomes integrable due to the conservation of momentum along the wire, the soft superconducting gap may arise naturally from the appearance of the trajectories with very long flight times due to their momentum being almost parallel to the nanowire axis [15, 10] [see Fig. 2.1(b)]. In a

simplified two-dimensional setup the flight time and the corresponding energy of the Andreev states are given by:

$$T(p_\parallel) = \frac{2m^* d}{\sqrt{p_F^2 - p_\parallel^2}}, \quad E_{\text{gap}} = \frac{\pi\hbar}{2T(p_\parallel)}, \tag{2.1}$$

with m^* the effective carrier mass, d the wire diameter, p_F the Fermi momentum, and $p_\parallel$ the momentum along the wire. Integration of $\rho(E)$ over $p_\parallel$ yields a linearly vanishing density of states near $E = 0$.

We have given this intepretation of the apparent soft gap in terms of a simplified 2D model. The argument depends on the flight time of classical paths, and hence depends sensitively on geometry. Directly applying this quasiclassical formalism to the 3D geometry of the experiment would only be possible numerically. Instead, we will present a full quantum calculation of the induced gap in the 3D nanowire geometry below. Still, we will be able to explain the main observed features in terms of this quasiclassical argument.

2.3 Methods and system setup

We consider a semiconducting nanowire with spin-orbit coupling, assuming that the spin-orbit coupling is due to a electric field perpendicular to the substrate. The nanowire Hamiltonian then reads:

$$\mathcal{H} = \frac{\mathbf{p}^2}{2m^*} + \frac{\alpha}{\hbar}(\sigma_x p_y - \sigma_y p_x) + E_Z\sigma_x + V(x), \tag{2.2}$$

where α is a parameter denotes the Rashba spin-orbit coupling strength, and $E_Z = \frac{1}{2}g\mu_B B$ is the Zeeman energy due to a magnetic field B in the x-direction, and $V(x)$ is a potential, e.g. due to disorder. In InSb, the effective mass $m^* = 0.014m_e$ where m_e is the bare electron mass, and $g = 51$.

We describe the presence of the superconducting contact within the Bogoliubov-de Gennes formalism, so that the total Hamiltonian for the semiconductor and the superconducting contact is given as

$$H_{BdG} = \begin{pmatrix} \mathcal{H} & \Delta \\ \Delta & -\mathcal{T}\,\mathcal{H}\,\mathcal{T}^{-1} \end{pmatrix}. \tag{2.3}$$

Here Δ is the superconducting order parameter, which we set nonzero only in the superconducting contact. Superconductivity in the nanowire is then only induced through proximity. $\mathcal{T}$ is the time-reversal operator.

In order to make contact to experiment and take into account the effects of broadening to to finite coupling to leads or finite temperature, we compute the Andreev conductance. To do so, we use the scattering matrix formalism. The scattering matrix for Andreev reflection reads

$$r_A = \begin{pmatrix} r_{ee} & r_{eh} \\ r_{he} & r_{hh} \end{pmatrix} . \tag{2.4}$$

where the individual blocks are the scattering matrices for reflection between electrons (e) and holes (h), respectively. The Andreev conductance is then given as

$$G = \frac{e^2}{h} \mathrm{Tr} \left(\mathbf{1} - r_{ee} r_{ee}^\dagger + r_{he} r_{he}^\dagger \right) . \tag{2.5}$$

We compute the scattering matrix (2.4) numerically in a tight-binding approximation of Eq. (2.3) using Kwant [16]. The geometry of the simulated system is shown in Fig. 2.1(a). In particular, we consider a nanowire with length $2\mu m$ and diameter $100\,nm$ coated by layer of superconductor (blue shell in Fig. 2.1(a)), covering an angle 2ϕ of the nanowire.

In the tight-binding description of the superconductor, we use the same hopping matrix element $t = \hbar^2/2ma^2$ (where a is the lattice constant of the discretization) as in the nanowire, and set $\Delta = t$, to be in the limit of short coherence length as appropriate for the superconductor used in the experiment [1]. The hopping t_s between superconductor and semiconductor is used as a fit parameter controlling the induced gap.

The proximitized part of the nanowire is separated from the normal part of the nanowire by a $25\,nm$ wide, rectangular tunnel barrier (red region in Fig. 2.1(a)). We tune the tunnel barrier height such that the normal state conductance $0.6\,e^2/h$.

We include random on-site disorder drawn from the uniform distribution $[-U_0, U_0]$. This random on-site potential itself does not have a physical meaning (the fluctations of the potential are on the scale of the lattice constant a of the discretization). To assess the strength of the disorder, we characterize it by computing the mean free path in a wire without magnetic field or superconductor.

We can extract the mean free path numerically from the disorder-

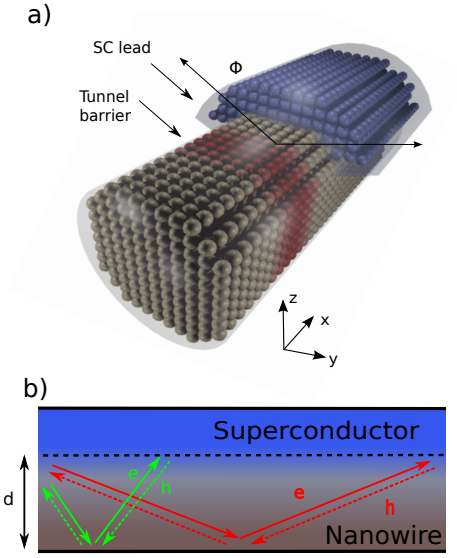

Figure 2.1. *a*) The layout of the system used in our study. The grey region indicates the nanowire, the blue shell the superconductor, and the red region shows the depleted part of the nanowire which forms the tunnel barrier. *b*) Schematic of paths for particles of different channels. The solid lines are trajectories of electrons and the dash lines of holes. The green lines indicates lower modes who have smaller parallel momentum thus shorter dwelling time and smaller and softer induced gaps. The red lines are for higher channel modes with larger parallel momentum and larger and harder induced gaps.

averaged conductance by fitting [17]

$$\langle G(\mu, U_0)\rangle = \frac{e^2}{h}\frac{N}{1+3L/4\xi_{\mathrm{MFP}}}, \tag{2.6}$$

where L is the length of the nanowire, and $\langle G\rangle$ the disorder averaged conductance.

The mean scattering time τcan also be computed from Fermi's golden rule, using the three-dimensional density of states of the nanowire bulk. We then find

$$\frac{1}{\tau} = \frac{a^3(2m^*)^{3/2}}{2\pi\hbar^4}\frac{1}{3}U_0^2\sqrt{\epsilon_F}, \tag{2.7}$$

where ϵ_F is the Fermi energy. The mean free path in our tight-binding

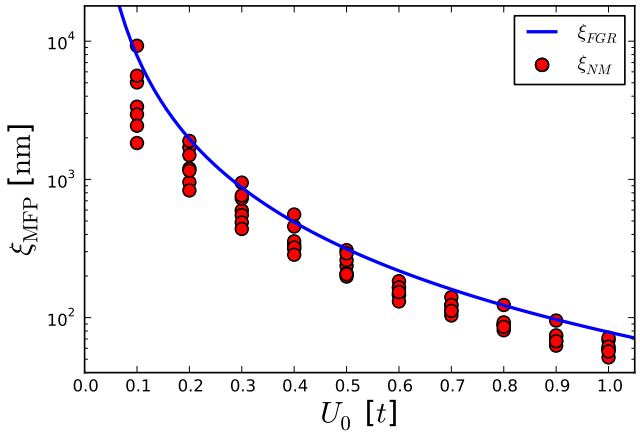

Figure 2.2. Mean free path ξ_{MFP} as a function of disorder strength U_0. Dots are numerically computed values for different values of chemical potential (corresponding to a range of 6–16 subbands) fitting disorder-averaged conductances for a range of nanowire lengths from 83 nm to 833 nm to Eq. (2.6). The solid line is the Fermi golden rule estimate from Eq. (2.8).

model from Fermi's golden rule is then given by

$$\xi_{\mathrm{MFP}} = v_F\,\tau = \frac{4\pi a}{\frac{1}{3}U_0^2/t^2} \tag{2.8}$$

In Fig. 2.2 we show both the numerically extracted mean free path as well as the prediction from Fermi's golden rule. Note that the latter does not account for the discrete subband structure of the nanowire, and correspondingly we observe a larger deviation from the numerical result for weak disorder, where subbands are mixed only little.

2.4 Gap softness

We first consider the induced superconducting gap in the nanowire in the absence of a magnetic field, $B = 0$. In this limit our general considerations relating classical paths to induced superconducting gaps are valid.

Since the induced gap depends inversely on the time between hits on the superconductor, we can expect the amount of surface being covered by the superconductor to have a large influence. In Fig. 2.3 we show

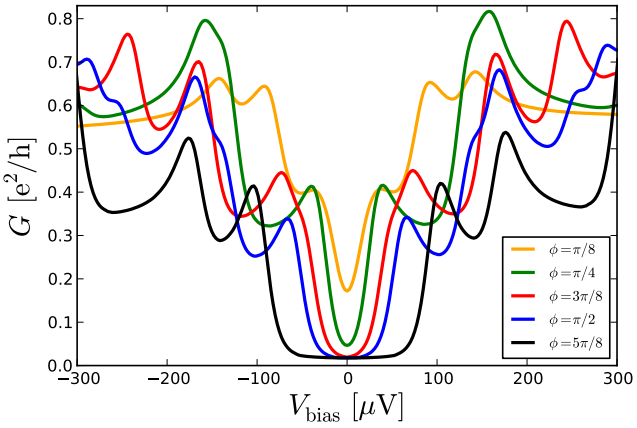

Figure 2.3. Influence of the coverage angle ϕ on the induced gap in the nanowire, as seen in the differential conductance G. Results are in the limit of a clean wire ($U_0 = 0$) and in the absence of a magnetic field ($B = 0$)

.

the differential conductance of the nanowire device as a function of bias voltage for different coverage angles ϕ of the superconductor.

A common feature for all coverage angles is that we observe not only a single superconducting gap, but instead a series of gaps, signaled by a series of coherence peaks with increasing bias voltage. We can attribute these to the different subbands that correspond to classical paths of different length, as argued above. The lowest subbands (with small transverse momentum) correspond to the smallest induced gaps, whereas the highest subbands (with a large transverse momentum) correspond to the largest induced gaps. In a clean system the conductances of the different modes simply add up. Thus we only see a strong suppression of the conductance within the smallest gap, whereas within the induced gap of the higher modes there is a finite conductance due to the above-gap conductance of the lower modes.

When increasing the coverage angle, we observe that each of the induced gaps increases monotonously. Again, this fits well with our expectations from the classical paths: For all modes the corresponding trajectories become shorter when the surface covered by the superconductor increases. A similar behavior is found when the coupling strength to the superconductor is changed (not shown here): When increasing the coupling strength, the probability of Andreev reflection is enhanced

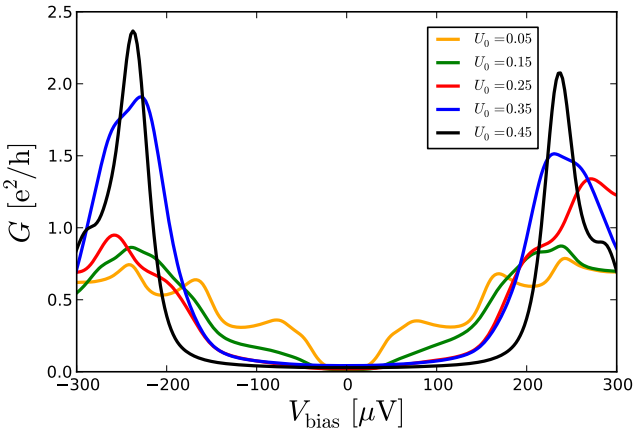

Figure 2.4. Influence of disorder on the observed gap in the conductance. Small disorder ($U_0 < 0.15$) reduces the observed coherence peaks and smoothens the observed gap. Larger disorder however leads eventually to a single hard gap. Results are for a coverage angle $\phi = 3\pi/8$, $t_s = t/2$ and zero magnetic field.

whereas the probability of normal reflection is reduced. This again leads to shorter trajectories and thus larger induced gaps for larger couplings.

The multi-mode nature of the nanowires thus leads naturally to a series of induced gaps, that manifest themselves in an increasing conductance until the bias voltage exceeds the largest induced gap. This is already reminiscent of the monotonously increasing sub-gap conductance in the experiment, if we identify the experimentally assigned gap with the largest induced gap in the highest subband. The main visual difference is the strong feature of a series coherence peaks in our numerics, that is absent in the experimental measurements. These strong coherence peaks for every subband are due to the fact that modes are globally well-defined in a clean system. Disorder will scatter between subbands and can thus have a large effect on the induced gaps.

For the remainder of the chapter we fix the coverage angle to $\phi = 3\pi/8$ in accordance with experiments [1]. We also fix $t_s = t/2$ to obtain a width of the apparent soft gap of 250 μeV as in the experiment, and continue to discuss the effects of disorder on the induced gap.

In Fig. 2.4 we show the dependence of the differential conductance on disorder strength. Weak disorder reduces the coherence peaks observed in the clean system due to scattering between subbands, and at $U_0 = 0.15$

only a smooth, soft gap is observed in the conductance, reminiscent of experiment. The presence of several modes in the nanowire together with weak scattering can thus explain the soft gap of the experiment completely.

For larger disorder strength, we instead find a transition to a single, hard gap. This is due to the fact that for strong scattering different modes are completely mixed, and the only remaining length scale in the problem is the mean free path. The latter is thus a natural cut-off for the maximum trajectory length and sets the value of the induced gap. The observation of a soft gap thus also sets an upper limit on the disorder present in the system. A comparison with Fig. 2.2 suggests a limit on the mean free path of order 1 μm. (It should be noted though that this estimate may depend on other details such as the potential drop across the nanowire.)

We note that the phenomenology observed here, a transition from a smooth gap to a hard gap with increasing disorder was described before for the case of metallic mesoscopic systems [14], where the semiclassical theory is expected to hold due to the large number of modes. Still, the semiclassical theory continues to describes the general trends in the semiconductor devices. Particular to our results is the prediction that in a clean nanowire system the different subbands would manifest themselves in series of coherence peaks. These should be observable in experiment if nanowire quality is improved.

2.5 Majorana zero-modes in a soft gap

Having established a plausible mechanism for an apparently soft gap in a proximitized nanowire, we now focus on the case of finite magnetic field, and in particular, Majorana zero-modes.

In a strictly one-dimensional wire a topological state with Majorana zero-modes is reached when [2, 3],

$$E_Z > \sqrt{\Delta^2 + \mu^2}\,. \tag{2.9}$$

In multi-band wires this condition still holds, provided that μ is replaced by $\mu - E_n$, where E_n is the band edge of the n-th subband [18]. In nanowires as typically used in experiments, the subband spacing is typically much larger than the Zeeman energy [19]. In this limit, only the

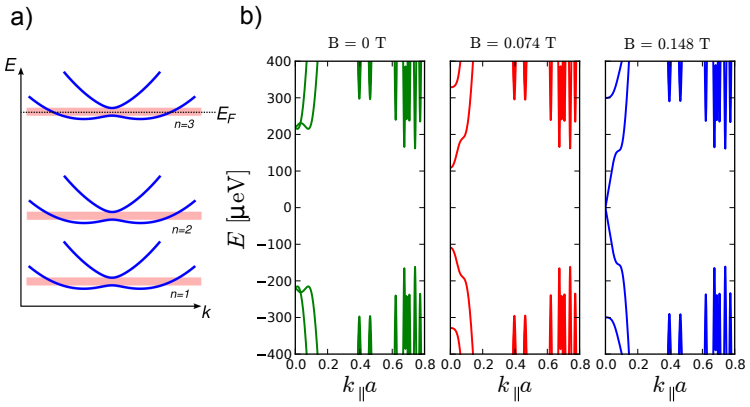

Figure 2.5. Majorana zero-modes in multi-band nanowires. (a) Schematic band structure of a multi-band nanowire with Rashba spin-orbit coupling in a magnetic field. A topological phase is reached if the Fermi energy E_F is tuned into the Zeeman gap of a subband; for a subband spacing larger than the Zeeman splitting this is only possible for the highest subband (with the largest confinement energy). (b) Band structure of proximitized nanowires for different values of the magnetic field. Results are for a coverage angle $\phi = 3\pi/8$ and $t_s = t/2$.

subband closest to the Fermi energy can be tuned into a topological state and host Majorana zero-modes [20, 21], as illustrated in Fig. 2.5(a) – the remainder of the subbands remains trivial.

The subband hosting an Majorana zero-mode hence has a large transverse momentum (the band edge being close to the Fermi energy), and hence a large induced gap. Hence, the Majorana zero-mode in proximitized nanowires are governed by the larger gap scale associated with the soft gap (in contrast to the smallest induced gaps of the lowest subbands). In particular, the threshold magnetic field for obtaining a topological state will be governed by this energy scale. This is in agreement with experiment [1], that have interpreted the largest energy scale of the soft gap as the induced gap Δ of the one-dimensional model Majorana theories [2, 3].

Figs. 2.5(b) show the band structure of a proximitized wire for increasing magnetic field. As expected from the previous arguments, only the highest mode (with the largest transverse momentum and the smallest longitudinal momentum k) shows a topological phase transition around

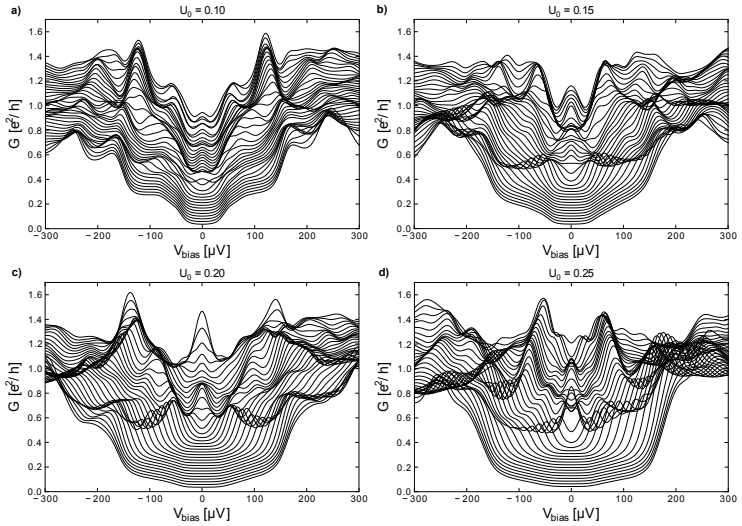

Figure 2.6. Andreev conductance of a proximitized nanowire for different disorder strengths ((a)-(d)) and different magnetic fields. Magnetic field is varied from $0 - 0.53\,\mathrm{T}$ and curves for different magnetic field are shifted vertically for clarity. Results are for a coverage angle $\phi = 3\pi/8$ and $t_s = t/2$.

$B = 0.15\,\mathrm{T}$. In fact, it is only this mode that shows an appreciable magnetic field dependence at all: All other subbands have a large longitudinal wave vector k_F and the spin-orbit energy $\alpha k_F \gg E_Z$, so that the induced gap for these modes is preserved in a magnetic field.

Hence, we find that in a clean wire the topological phase transition involves a single subband only, whereas the remainder of the modes forms an magnetic-field independent background. We can thus expect a similar phenomenology in the transport as was discussed for a constant induced gap common to all modes [20, 21], i.e. the appearance of a zero-bias peak in a background of a nearly magnetic-field independent gap and with a low visibility of the gap closing at the topological phase transition. The main difference to this previous work is that we now find the zero bias peak in apparently soft gap.

This expectation is confirmed by numerical calculations. In Fig. 2.6(a) we show the numerically calculated Andreev conductance for a range of magnetic field for weak disorder. In this case indeed the zero-bias peak appears without the topological phase transition visible as a gap closing. In addition, the series of induced gaps is visible as a constant background,

independent of magnetic field, and the remnants of the coherence peaks is visible as a series of nearly magnetic-field independent peaks at different bias voltages. We predict that these should be also visible in experiment as nanowire quality improves.

When disorder is increased, the visibility of the coherence peaks vanishes, and the gap is softened even more (Fig. 2.6(b)). In this case also the visibility of the gap closing at the topological transition increases, though the degree of softness and the onset of a visible gap closing depend very much on the details of the disorder and the barrier, i.e. a soft gap does not automatically imply that the gap closing should be visible. When disorder is increased more (Figs. 2.6(c),(d)), the induced gap becomes hard, but is also more strongly affected already by weak magnetic fields. In this case the superconducting gap starts to close at similar field strength required for the Majorana zero-mode to form. For even stronger disorder we find the gap to close completely with a number of low-energy states forming a large zero-bias peak as described in [22].

2.6 Conclusion

Our main finding is that a multichannel nanowire with limited scattering naturally exhibits an apparently soft gap. This is due to different induced superconducting gaps in each of the different channels. Disorder mixes subbands and ultimately leads to a single, hard induced gap. The observation of a soft gap thus may pose an upper limit on the scattering in nanowires.

The appearance of Majorana zero-modes is not affected significantly by the apparently soft gap. In fact, Majorana zero-modes are governed by the largest induced gap in the nanowire - this is advantageous for their observation as the corresponding coherence length of the topological gap scales inversely with the induced s-wave gap. A shorter coherence length protects Majorana zero-modes from disorder and separates the Majorana zero-modes at the two ends of the nanowire. On the other hand, the presence of the small induced gaps constituting the soft gap in the nanowire implies a very much smaller energy scale for other quasiparticles in the system. This may be a serious obstacle for observing the braiding statistics of Majorana zero-modes.

Our proposed mechanism for the soft gap has consequences that can be tested experimentally: First, we predict that in clean nanowires the An-

dreev conductance exhibits a series of nearly magnetic-field independent peaks corresponding to the induced gaps in the different subbands. Second, we predict that due to the small energy scale of the smallest induced gap there should be a significant normal transconductance between the two ends of the nanowire.

Bibliography

[1] V. Mourik, K. Zuo, S. M. Frolov, S. R. Plissard, E. P. A. M. Bakkers, and L. P. Kouwenhoven, Science **336**, 1003 (2012).

[2] R. M. Lutchyn, J. D. Sau, and S. Das Sarma, Phys. Rev. Lett. **105**, 077001 (2010).

[3] Y. Oreg, G. Refael, and F. von Oppen, Phys. Rev. Lett. **105**, 177002 (2010).

[4] M. T. Deng, C. L. Yu, G. Y. Huang, M Larsson, P. Caroff, and H. Q. Xu, Nano Lett. **12**, 6414 (2012).

[5] A. Das, Y. Ronen, Y. Most, Y. Oreg, M. Heiblum, and H. Shtrikman, Nature Phys. **8**, 887 (2012).

[6] L. P. Rokhinson, X. Liu, and J. K. Furdyna, Nat. Phys. **8**, 795 (2012).

[7] D. I. Pikulin, J. P. Dahlhaus, M. Wimmer, H. Schomerus, and C. W. J. Beenakker, New J. Phys. **14**, 125011 (2012).

[8] H. O. H. Churchill, V. Fatemi, K. Grove-Rasmussen, M. T. Deng, P. Caroff, H. Q. Xu, and C. M. Marcus, Phys. Rev. B **87**, 241401 (2013).

[9] G. E. Blonder, M. Tinkham, and T. M. Klapwijk, Phys. Rev. B **25**, 4515 (1982).

[10] P. G. de Gennes and D. Saint-James, Phys. Lett. **4**, 151 (1963).

[11] P. W. Anderson, J. Phys. Chem. Solids **11**, 26 (1959).

[12] S. Takei, B. M. Fregoso, H.-Y. Hui, A. M. Lobos, and S. Das Sarma, Phys. Rev. Lett. **110**, 186803 (2013).

[13] T. D. Stanescu, R. M. Lutchyn, and S. Das Sarma, Phys. Rev. B **90**, 085302 (2014).

[14] S. Pilgram, W. Belzig, and C. Bruder, Phys. Rev. B **62**, 12462 (2000).

[15] C. W. J. Beenakker, Lect. Notes. Phys. **667**, 131 (2005).

[16] C. W. Groth, M. Wimmer, A. R. Akhmerov, and X. Waintal, New. J. Phys. **106**, 127001 (2001).

[17] C. W. J. Beenakker, Rev. Mod. Phys. **69**, 731 (1997).

[18] R. Lutchyn, T. Stanescu, and S. Das Sarma, Phys. Rev. Lett. **106**, 127001 (2011).

[19] I. van Weperen, S. R. Plissard, E. P. A. M. Bakkers, S. M. Frolov, and L. P. Kouwenhoven, Nano Lett. **13**, 387 (2013).

[20] T. Stanescu, S. Tewari, J. Sau, and S. Das Sarma, Phys. Rev. Lett. **109**, 266402 (2012).

[21] F. Pientka, G. Kells, A. Romito, P. Brouwer, and F. von Oppen, Phys. Rev. Lett. **109**, 227006 (2012).

[22] J. Liu, A. C. Potter, K. T. Law, and P. A. Lee, Phys. Rev. Lett. **109**, 267002 (2012).